Heliyon 5 (2019) e02843

Contents lists available at ScienceDirect

Heliyon

journal homepage: www.heliyon.com

Heliyon

Research article

Melt spinnabilities of thermoplastic paramylon mixed esters

Motonari Shibakami [a,*], Mitsugu Sohma [b], Norihito Kijima [b], Tadashi Nemoto [a]

[a] Biomedical Research Institute, National Institute of Advanced Industrial Science and Technology (AIST), Central 6th, 1-1-1 Higashi, Tsukuba, Ibaraki, 305-8566, Japan
[b] Advanced Coating Technology Research Center, National Institute of Advanced Industrial Science and Technology (AIST), Central 5th, 1-1-1 Higashi, Tsukuba, Ibaraki, 305-8565, Japan

ARTICLE INFO

Keywords:
Organic chemistry
Materials chemistry
Melt spinning
Paramylon mixed ester
Euglena
Thermoplasticity
Monofilament

ABSTRACT

The low thermoplasticities of polysaccharide esters make them unsuitable for melt spinning. In this study, we aimed to overcome this problem by mixed esterification of paramylon, a euglenoid β-1,3-glucan with short- and medium-chain acyl groups, as melt-spinnable materials. Thermal analyses revealed that all the synthesized paramylon mixed esters exhibited glass transition temperatures greater than 100 °C; some of them showed large differences between the melting and 5%-weight-loss temperatures (*Td*5s) and are extrudable through a spinneret at a temperature ~100 °C below *Td*5, rendering them potential candidates for the production of melt-spun filaments. Among the various compounds investigated, paramylon acetate propionates, in which the degrees of acetyl- and propionyl-group substitution were 0.5–0.7 and 2.2–2.5, respectively, could be melt-spun to yield mechanically tough crystalline monofilaments. In contrast, the melt spinning of cellulose acetate propionate, analogous to the paramylon acetate propionates in terms of acyl substituents, their substitution degrees, and molecular weights, but differs from it in terms of the glucose linkage mode (i.e., β-1,3 vs β-1,4), yielded brittle, charred, and short filaments. Curdlan acetate propionate, another analogue with a degree of polymerization five times larger than that of paramylon mixed esters, was not extrudable due to the lack of thermoplasticity. Therefore, we herein confirmed the superiority of paramylon as a primary raw material for melt-spun filaments.

1. Introduction

Thermoforming is a useful technique for molding products of various forms from thermoplastic polymers (Throne, 2008). Owing to depletion of global petroleum reserves, there is increasing interest in replacing petroleum-based thermoplastics with those derived from renewable resources. Unfortunately, polysaccharides are unsuitable for this purpose because they do not exhibit the desired degree of thermoplasticity; hence, polysaccharides need to be chemically modified (Erdmann et al., 2014; Zepnik et al., 2013). Acylation with a short-chain fatty acid, such as acetic acid, is a typical method used to chemically modify cellulose, the most abundant natural polysaccharide. However, the narrow process window, which ranges from the melting temperature to the decomposition temperature, prevents successful thermoforming of thermoplastic acylated cellulose derivatives. This necessitates the use of a large amount of plasticizer, which can reduce the mechanical strength and heat resistance of the final product (Park et al., 2004; Toyama et al., 2015). The aforementioned problem is encountered in melt spinning, a thermoforming technique for producing monofilaments, as well as in other techniques, particularly when an acylated cellulose derivative is used as the raw material. To circumvent this problem, a combination of cellulose mixed esters (cellulose acetate propionates (CAPs) and cellulose acetate butyrates (CABs)) and a water-washable plasticizer have been employed (Aranishi et al., 2006). Hooshmand et al. prepared continuous fibers based on CAB using cellulose nanocrystals and triethyl citrate as additives, in order to improve the mechanical strength and thermoplasticity (Hooshmand et al., 2014). Although these thermoforming methods are efficient, they render the production process more complex. Both CAP and CAB are commercially available and commonly used thermoplastic cellulose mixed esters. Given that the thermoplasticity of a CAP likely stems from its lower degree of polymerization (DP) (= M_w/molecular weight of acyl-substituted glucose unit), which ranges from ~140 to 300, as well as mixed esterification (Aranishi et al., 2006), we hypothesized that there is room to improve these mechanical properties. Owing to the high hydroxyl group contents of CABs (4.8 wt%), which enables their dissolution in alcohols (Hooshmand et al., 2014), we also expected cellulose mixed-ester-based monofilaments to show low alcohol and water resistances. We believe that these potential issues are inherent to the use of cellulose.

Our approach to the preparation of polysaccharide-based

* Corresponding author.
E-mail address: moto.shibakami@aist.go.jp (M. Shibakami).

https://doi.org/10.1016/j.heliyon.2019.e02843
Received 19 February 2019; Received in revised form 17 July 2019; Accepted 8 November 2019

monofilaments through melt spinning involves the use of paramylon, a linear β-1,3-glucan from *Euglena*, as the main chain of the thermoplastic polysaccharide. We expected paramylon mixed esters to exhibit better thermoplasticity during melt spinning than cellulose, a β-1,4-glucan, upon chemical modification, because of the following reasons. First, the narrow polymer chain-length distribution of paramylon (polydispersity index = weight-average molecular weight (M_w)/number-average molecular weight (M_n) ≈ 1.2) would cause its derivatives to melt within a small temperature range. Second, there are large differences (~100 °C) between the melting (T_m) and the 5%-weight-loss temperatures ($Td5$s) of paramylon acetate propionate, paramylon acetate butyrate, paramylon acetate pentanoate, and paramylon acetate hexanoate. Such temperature difference facilitates melting of the paramylon mixed esters without charring (Shibakami and Sohma, 2017). Third, we expected that the linear polymeric structures of β-1,3-glucans facilitate greater degree of thermoplasticization than the structurally analogous β-1,4-glucans, such as cellulose, because they prevent excessive polymer entanglement. Alternatively, the polymer chains exhibit well-ordered alignment in the solid state owing to the helicity of the β-1,3-bond. Fourth, paramylon is more favorable as a backbone of thermoplastics than curdlan, a structurally analogous β-1,3-glucan, because its molecular weight, which is three times larger than that of paramylon, obstructs thermoplasticization (Shibakami and Sohma, 2017). Therefore, we hypothesized that thermoplastic paramylon mixed esters can be transformed into mechanically tough monofilaments more readily than the structurally analogous β-1,4-glucans and curdlan if their physical properties, such as surface tension, viscosity, and elasticity in the molten state, and spinning conditions including temperature, extruding force, and speed, are balanced for melt spinning (Nakagawa, 1952a, 1952b).

The main purpose of this study was to elucidate the chemical structures of thermoplastic paramylon mixed esters that exhibit balance between thermoplasticity for melt spinnability and ability to form mechanically tough filaments. In this study, cellulose acetate propionate, curdlan acetate propionate, and eleven candidate paramylon mixed esters, with different acyl chain lengths, acyl group degrees of substitution (DS), and acyl group combinations, were synthesized. Their structural and thermal properties were then characterized. Candidates for melt-spun filament materials chosen from among these compounds via preliminary manual melt spinning were paramylon acetate propionates having low acetyl DS and high propionyl DS. We confirmed that the compounds are transformable to monofilaments via mechanical melt spinning. The mechanical, thermal, and X-ray diffraction analyses indicate that these filaments are crystalline in character and their mechanical properties are comparable to those of practically used cellulose-based filaments. The advantages of melt spinning that is applicable to the melt spinnable paramylon mixed esters include the non-use of hazardous solvents and plasticizers that are necessary for producing conventional cellulosic filaments, including viscose rayon and cellulose acetate (Teramoto, 2015).

2. Experimental

2.1. General methods

The ^{1}H and ^{13}C nuclear magnetic resonance (NMR) spectra of the products were obtained using a Bruker AVANCE 500 spectrometer (500 MHz). The Fourier-transform infrared (FT-IR) spectra of the thin films of polysaccharide mixed ester solids formed by hot pressing (~50 mg, 230 °C, 10 MPa, 10 s) were obtained using a JASCO FT/IR-480ST spectrophotometer equipped with an attenuated total reflectance accessory (ZnSe prism, ATR Pro 400-S, JASCO) with a resolution of 4 cm^{-1}. The DS, which is defined as the average number of functional groups attached to a glucose unit, was determined by comparing the integrated value of methyl/methylene protons of the medium-chain acyl and acetyl groups with that of the glucose protons in the ^{1}H NMR spectrum; DS_{ace} and DS_{mc} represent the DS values of the acetyl and medium-chain acyl groups (i.e., propionyl, butanoyl, pentanoyl, and hexanoyl), respectively. All the chemicals and reagents were obtained commercially and were used without purification. Paramylon was obtained from *Euglena gracilis* strain EOD-1 (FERM BP-11530). The ^{1}H NMR, ^{13}C NMR, and FT-IR data, and the M_w and M_n of paramylon are as follows: ^{1}H NMR (1.0 M NaOD/D_2O) δ 4.72 (m, 1H; H1), 3.93–3.45 (m, 6H; H2–H6); ^{13}C NMR (1.0 M NaOD/D_2O) δ 106.3 (C1), 89.9 (C3), 79.6 (C5), 76.6 (C2), 72.3 (C4), 64.1 (C6); FT-IR (cm^{-1}) 3361, 2899, 1118, 1078, 1040, 885; $M_w = 1.892 \times 10^5$ and $M_n = 1.531 \times 10^5$ (Shibakami and Sohma, 2017). Dissolving pulp (α-cellulose ˃92%, NDPS, estimated $M_w = 3.285 \times 10^5$ (Shibakami and Sohma, 2017)) was obtained from Nippon Paper Industries Co., Ltd. Curdlan was purchased from FUJIFILM Wako Pure Chemical Corporation. Cellulose acetate butylate (M_n: ~30,000) (CAB) was purchased from Sigma-Aldrich. The DS_{ace}, DS_{mc}, T_g, M_w, and M_n of CAB determined herein are 0.36, 2.64, 97.1 °C, 5.298 × 10^4 (3), and 3.626 × 10^4 (3), respectively.

2.2. Synthesis of paramylon mixed esters

Paramylon mixed esters (products **1a**–**1d**, **2**, **3**, **4a**, **4b**, **5**–**7**) were synthesized according to our previously reported method (Shibakami and Sohma, 2017). The procedure, as well as that for the syntheses of cellulose acetate propionate (product **8**) and curdlan acetate propionate (product **9**), is described in the Supplementary Material.

2.2.1. Paramylon acetate propionate from acetic acid and propionic anhydride (1a) (feed molar ratio = 1:3)

A mixture of paramylon (15.007 g, 92.56 mmol), LiCl (11.738 g, 276.90 mmol), and *N*,*N*-dimethylacetamide (DMAc) (750 mL) was heated at ~100 °C for ~0.5 h under nitrogen. To the resulting homogeneous solution, 4-dimethylaminopyridine (2.159 g, 17.67 mmol) was added in a single portion. Subsequently, a solution prepared by heating a mixture of acetic acid (12.590 g, 204.66 mmol) and propionic anhydride (81.391 g, 625.41 mmol) at ~110 °C for 1 h under nitrogen was added dropwise. After stirring the reaction mixture at ~100 °C for 3 h, methanol (750 mL) was added. The mixture was then added dropwise to water (3.0 L), resulting in the formation of a white precipitate. This precipitate was separated by decantation and dispersed in chloroform (500 mL), and the heterogeneous mixture was stirred overnight using a mechanical stirrer at ambient temperature. After removing the aqueous layer, the nearly homogeneous mixture was poured into ethanol (1.5 L) to obtain a white precipitate. This precipitate, and the one produced by allowing the ethanol solution to stand overnight, were combined, dispersed in chloroform (350 mL), and mechanically stirred at ambient temperature overnight. The resulting homogeneous solution was poured into ethanol (1.5 L) to yield a white precipitate. This purification process was repeated twice. Air drying overnight and vacuum drying (~60 °C, 8 h) yielded the desired product (**1a**) as a white solid (25.268 g, 77.54 mmol, Yield: 84.3%). The successful synthesis of **1a** was confirmed by ^{1}H NMR and FT-IR spectroscopies: ^{1}H NMR ($CDCl_3$) δ 4.86 (brs), 4.80 (brs), 4.29 (brs), 4.02 (brs), 3.71 (brs), 3.59 (brs), 2.51–1.99 (m), 1.18–1.09 (m); DS_{ace}, 0.46; DS_{mc}, 2.54; ^{13}C NMR ($CDCl_3$) δ 174.0, 172.5, 172.3, 170.6, 169.1, 168.9, 100.7, 78.2, 72.7, 72.2, 68.1, 62.1, 27.3, 20.7, 8.9; FT-IR (cm^{-1}) 2976, 1735, 1363, 1154, 1045, 1014, 870, 807.

2.3. Size exclusion chromatography

The polysaccharide mixed esters were subjected to size exclusion chromatography using a gel permeation chromatography column (KD-805, Shodex) (elution solvent: chloroform, elution temperature: 40 °C, elution solvent flow rate: 1.0 mL/min). The chromatography system was equipped with a multi-angle static light-scattering set-up combined with a multi-angle laser photometer (miniDAWN, Wyatt Technology), a dynamic light-scattering module (WyattQELS, Wyatt Technology), and a refractive index detector (Optilab rEX, Wyatt Technology). The solutions for analysis were prepared by dissolving the polysaccharide mixed esters

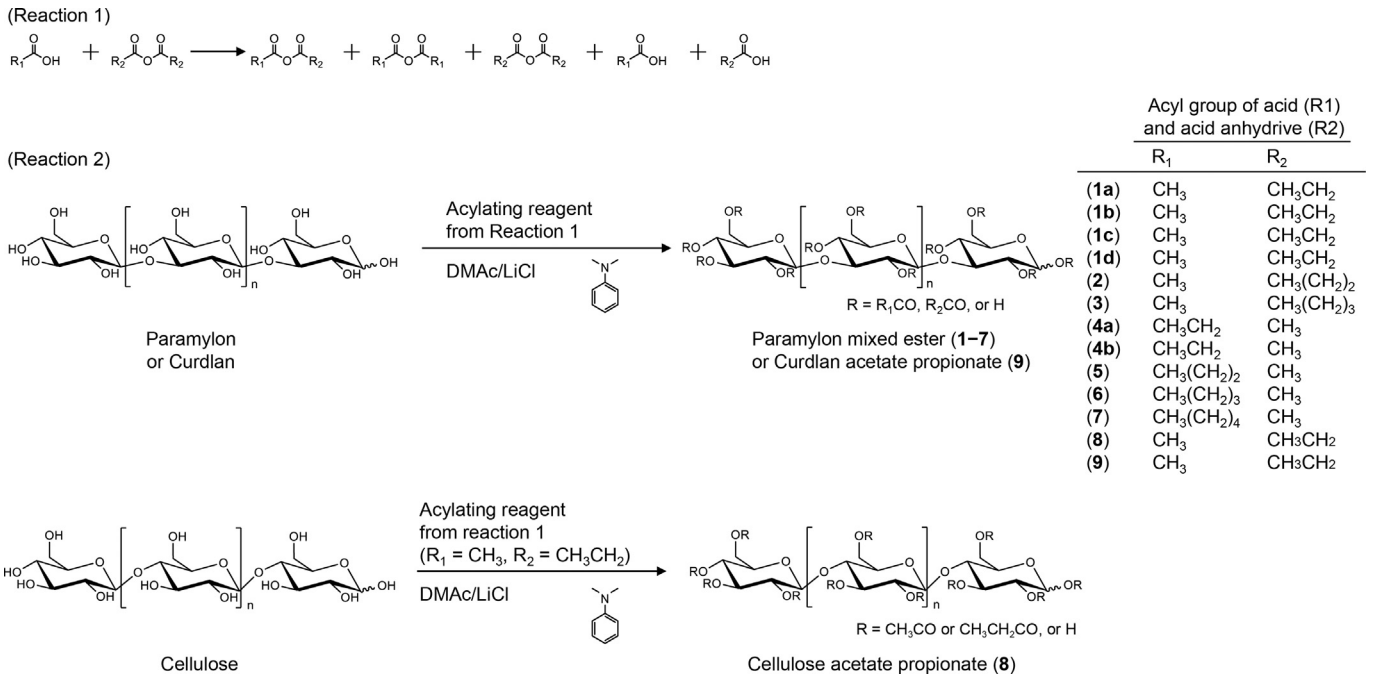

Scheme 1. Reactions involved in synthesis of polysaccharide mixed esters.

in chloroform and purified through a 0.20-μm filter prior to injection. The concentration was ~4.0 mg/mL, the injection volume was 100 μL, and the refractive index increment (*dn/dc*) was 0.0372.

2.4. Thermal analysis

The melting behavior of the ethanol-precipitated solids was preliminarily observed using a melting point apparatus (MP-500D, Yanako). The T_m, glass transition temperature (T_g), and enthalpy change (ΔH) were determined from the differential scanning calorimetry (DSC) thermograms obtained using a calorimeter (Thermo plus EVO2 DSC 8230, Rigaku). Each ethanol-precipitated solid (~6 mg) was mechanically sealed in an aluminum pan and heated from 25 to 230 °C (10.0 °C/min) and held at 230 °C for 3 min. After cooling from 230 to 25 °C (5.0 °C/min) and holding at 25 °C for 5 min, the test sample was heated to 250 °C at the same scan rate. The thermogram obtained during the first heating step was used to determine T_m, whereas that obtained during the second heating step was used to determine T_g and ΔH. Furthermore, thermogravimetric analysis was performed on the ethanol-precipitated solids using a thermogravimetric (TG) analyzer (Thermo plus EVO2 TG 8120, Rigaku) to determine the *Td*5 value. Each sample was heated from 25 to 500 °C (10.0 °C/min) under flowing nitrogen (100 mL/min). Isothermal stability of the ethanol-precipitated solids was evaluated using thermogravimetric analysis, in which the sample weight was continuously measured upon isothermal heating (246 ± 1.0 °C, 30 min). To obtain the thermal properties of the melt-spun filaments, they were subjected to DSC analysis using the same heating/cooling program used for the ethanol-precipitated solids.

2.5. Melt volume flow rate (MVR) measurements

MVR measurements were performed using a melt indexer (IMC-E0F0, Imoto). Briefly, ~1.0 g of the polysaccharide mixed ester solid was placed in the cylinder (length of 100 mm, and outer and inner diameters of 50.0 and 7.0 mm, respectively) of the melt indexer and heated at different temperatures (210, 220, 230, 240, and 250 °C) for 3 min. The melted solid was then extruded from the cylinder through a die orifice (length of 10 mm, and outer and inner diameters of 7.0 and 1.0 mm, respectively) using a 37.26-, 49.03-, or 98.07-N weight. The MVR was calculated by measuring the volume of the solid extruded through the orifice.

$$\text{MVR (cm}^3\text{/10 min)} = (A \times t_{ref} \times L)/t, \quad (1)$$

where A is the cross-sectional area of the orifice (0.407 cm^2), t_{ref} is the base time (600 s), L is the stroke length of the piston (1.25 cm), and t is the stroke time of the piston (*s*).

2.6. Melt spinning

Melt spinning was performed using a custom-built spinning system comprising the melt indexer (IMC-E0F0, Imoto) used for MVR measurement and a spinning apparatus (IMC-1128, Imoto). Briefly, ~1.0 g of the solid polysaccharide mixed ester was placed in the cylinder and heated at different temperatures (160, 240, 245, and 250 °C) for 3 min. The melted solid was then extruded from the cylinder through a spinneret (same as the orifice for melt spinning) using a 37.26- or 98.07-N weight. The extruded monofilament was quickly air-cooled and spun using the spinning apparatus with a roll of diameter 90 mm (mechanical spinning) or by hand (manual spinning).

The monofilament fineness (in dtex) was determined by dividing the length of the filament by its weight.

2.7. Mechanical strength measurements

Tensile tests were performed on the melt-spun monofilaments using a universal tester (Tensilon RTG-1225, A&D) at room temperature. The initial distance between the chucks was set at 30 mm, and the pulling rate was 3 mm/min. The number of samples tested in each case was more than 50.

2.8. Scanning electron microscopy (SEM)

The monofilaments were fixed on the metal stage of the microscope using a carbon conductive double-sided tape. Images were acquired under high vacuum using a scanning electron microscope (JSM-6060, JEOL) operated at an accelerating voltage of 2.5 kV.

Table 1
Polymeric structural parameters of polysaccharide mixed esters.

Product	R_1	R_2	Feed molar ratio of A/AA	DS_{ace}	DS_{mc}	M_w ($\times 10^5$)	M_n ($\times 10^5$)	M_w/M_n	DP
1a	CH_3	CH_3CH_2	1/3	0.46	2.54	4.615 (0.8)[a]	3.504 (0.8)	1.317 (1.0)	1416
1b	CH_3	CH_3CH_2	1/2	0.72	2.24	4.680 (0.8)	3.561 (1.0)	1.314 (1.0)	1462
1c	CH_3	CH_3CH_2	1/1	1.03	1.96	3.990 (1.0)	3.174 (2.0)	1.257 (3.0)	1257
1d	CH_3	CH_3CH_2	2/1	1.50	1.25	5.029 (0.5)	3.938 (0.6)	1.277 (0.7)	1692
2	CH_3	$CH_3(CH_2)_2$	1/1	1.24	1.71	4.467 (0.4)	3.628 (0.5)	1.568 (1.0)	1329
3	CH_3	$CH_3(CH_2)_3$	1.2/1	1.24	1.73	5.042 (0.8)	3.957 (2.0)	1.274 (2.0)	1394
4a	CH_3CH_2	CH_3	1/2	1.82	0.90	4.148 (0.7)	3.178 (1.0)	1.305 (1.0)	1364
4b	CH_3CH_2	CH_3	2/1	1.20	1.33	3.293 (1.0)	2.321 (2.0)	1.419 (3.0)	1146
5	$CH_3(CH_2)_2$	CH_3	1/1	2.32	0.65	3.642 (0.4)	3.007 (0.6)	1.211 (0.7)	1029
6	$CH_3(CH_2)_3$	CH_3	1/2	2.52	0.41	5.156 (0.5)	4.348 (0.5)	1.186 (0.7)	1311
7	$CH_3(CH_2)_4$	CH_3	1/2	2.52	0.45	3.615 (0.4)	3.109 (0.5)	1.333 (1.0)	840
8	CH_3	CH_3CH_2	1/3	0.54	2.46	5.671 (4.0)	2.527 (2.0)	2.244 (5.0)	1746
9	CH_3	CH_3CH_2	1/3	0.40	2.46	25.47 (4.0)	21.66 (5.0)	1.176 (7)	7925
CAB	CH_3	$CH_3(CH_2)_2$	–	0.36	2.64	0.5298 (3)	0.3626 (3)	1.461 (4)	145

A, acid; AA, acid anhydride.
[a] Values in parentheses indicate percentage errors.

2.9. Wide-angle X-ray diffraction (WAXD)

WAXD experiments were performed using an X-ray diffractometer (RINT-2550V, Rigaku) with monochromatic Cu-Kα radiation (λ = 0.15418 nm) generated at 40 kV and 200 mA through an optical slit system (divergence slit angle = 0.5°, scattering slit angle = 0.5°, and receiving slit = 0.3 mm). Scattering was performed over the scattering angle (2θ) range 2–60° at a step size of 0.05° and scan rate of 5°/min.

2.10. Dynamic mechanical analysis (DMA)

DMA was performed on the monofilaments (length = 20 mm, diameters = 176, 153, and 113 μm) using a dynamic mechanical analyzer (RSA-G2, TA Instruments). The dynamic moduli of the monofilaments were measured at 0.1% strain and 1 Hz from 30 to 150 °C at a heating rate of 5 °C/min. The axial force was adjusted to 0.15 N, and a strain adjust of 15% was set with a minimum strain of 0.01%, maximum strain of 1%, and minimum force of 0.01 N to prevent the samples from

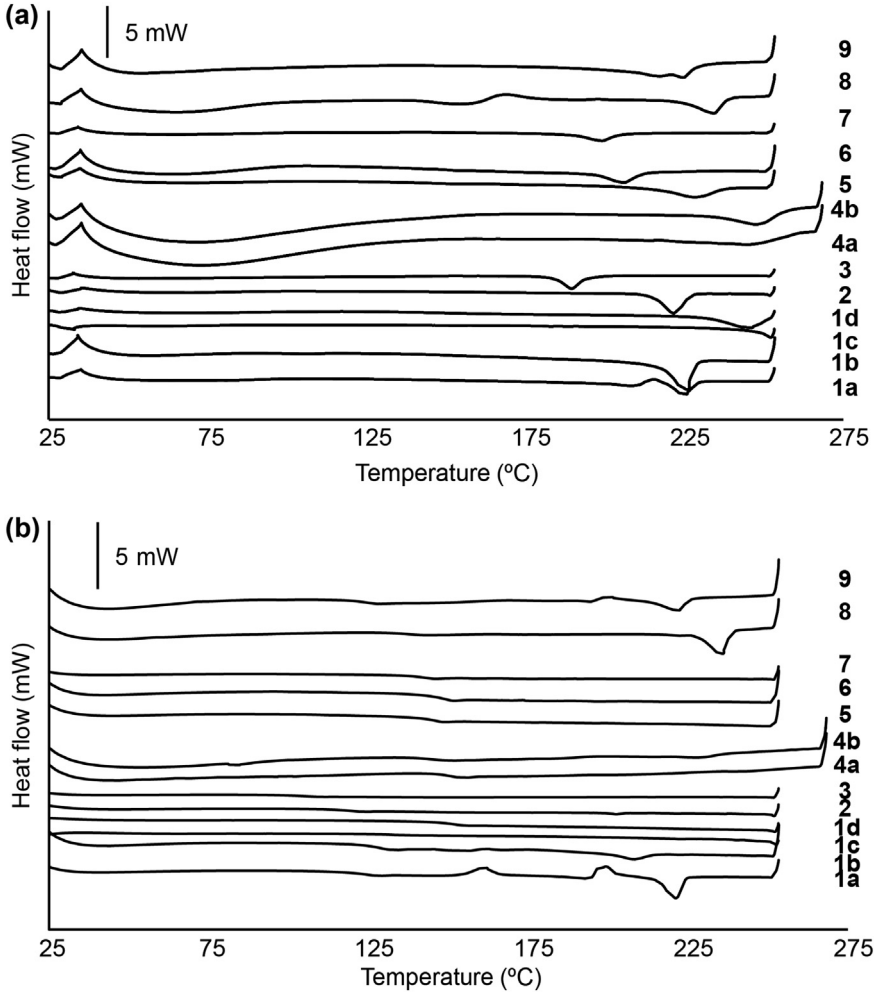

Fig. 1. DSC thermograms of ethanol-precipitated polysaccharide mixed esters: (a) first and (b) second heating scans.

buckling or exceeding the specified strain. A force tracking mode was set such that the axial force was thrice the magnitude of the oscillation force.

3. Results and discussion

3.1. Design and synthesis of paramylon mixed esters

For polysaccharide esters, the thermoplasticization and reinforcing effects of acylation exhibit an inverse relationship, i.e., the longer the acyl chain, the higher is the thermoplasticization effect but the lower is the mechanical strength of the final product (Marubayashi et al., 2014; Puanglek et al., 2017). Hence, the primary objective of this study was to determine the combination of length, DS range, and acyl group that would make the paramylon thermoplasticity suitable for melt spinnability and endow it with the ability to form mechanically robust monofilaments that circumvent the need for plasticizers. With this goal in mind, we synthesized eleven paramylon mixed esters with varying combinations of two acyl groups and DS values.

The reactions involved in the synthesis of the paramylon mixed esters, **8**, and **9** are modified versions of previously reported reactions (Shibakami and Sohma, 2017) (Scheme 1). All the products contain an acetyl group as the shorter chain because substitution with the smallest acyl group (the acetyl group) contributes to mechanical robustness. At the same time, this substitution reduces thermoplasticity. However, thermoplasticity for melt spinnability and mechanical toughness of filaments can be simultaneously achieved if the chain length and DS of the medium-chain acyl groups are optimized. Briefly, a mixture of acid anhydrides is produced by the reaction between a fatty acid (acetic, propionic, butyric, pentanoic, or hexanoic acid) and an acid anhydride (acetic, propionic, butyric, or pentanoic anhydride) (Reaction 1). The acid anhydrides then react with either paramylon, cellulose from dissolving pulp, or curdlan to yield products **1**–**9** (Reaction 2). Specifically, paramylon was treated with acid anhydrides obtained from a mixture of acetic acid and propionic anhydride (**1a–1d**) or propionic acid and acetic anhydride (**4a**, **4b**), at different molar feed ratios, to produce paramylon acetate propionates having various DS values. Since the content ratio of the acylating reagent (acid anhydride) depends on the combination of the fatty acid and acid anhydride as well as the corresponding molar feed ratio, these synthesis conditions should provide paramylon acetate propionates with a wide variety of DS values. We anticipated that these products would be the most promising candidates because they contained the shortest and the second-shortest acyl groups.

Table 1 shows the DS values of the synthesized products and CAB. As expected, those of the paramylon acetate propionates (**1a**−**1d**, **4a**, **4b**) vary widely; specifically, 0.46–1.82 for DS_{ace} and 0.90–2.54 for DS_{mc}. Both paramylon acetate butyrates **2** and **5**, and paramylon acetate pentanoates **3** and **6** have two different DS combinations: medium-chain-acyl-rich (**2**, **3**) and acetyl-rich (**5**, **6**). The acetyl-rich paramylon acetate hexanoate (**7**), **8,** and **9** were prepared for comparison; **7** had DS values comparable to those of **5** and **6**, whereas **8** and **9** had DS values comparable to those of **1a**.

Table 1 also shows the molecular weights and DPs of the products. The M_w and M_n of the paramylon mixed esters ranged from ~3.3×10^5 to ~5.2×10^5 and from ~2.3×10^5 to ~4.3×10^5, respectively. The M_w and M_n of **8** were comparable to these values and those of **9** were 5−6-times larger than those of **1a**. CAB used herein has lower molecular weights. The M_w/M_n (i.e., polydispersity index) of the paramylon mixed esters ranged from ~1.2 to ~1.6, indicating that esterification did not significantly change the inherent near-monodispersity of paramylon (≈1.2). The M_w/M_n of **8** was higher than those of the paramylon mixed esters because of the successive harsh extraction, purification, and fibrillation processes employed in the preparation of dissolving pulp (Savage et al., 1954), while the M_w/M_n of **9** was comparable to those of the paramylon mixed esters. The DPs of the paramylon mixed esters ranged from ~840 to 1700, higher than those of the CAB used herein and the CABs used for previously reported melt spinning studies (Aranishi et al., 2006).

Table 2
Thermal properties of polysaccharide mixed esters.

Product	T_m (°C)	*Td*5 (°C)	*Td*5– T_m (°C)	Weight loss (%)	T_g (°C)
1a	225.4	344.9	119.5	-0.50	120.7
1b	225.1	342.7	117.6	-0.30	125.7
1c	252.1	338.9	86.8	-0.28	132.4
1d	245.0	274.8	29.8	-1.05	149.7
2	221.9	345.6	123.7	-0.34	116.5
3	189.9	348.7	158.8	-0.22	102.5
4a	244.8	203.9	-40.9	-2.37	150.1
4b	247.3	221.3	-26.0	-1.90	147.8
5	228.1	340.5	112.4	-0.15	142.6
6	205.9	327.8	121.9	-0.67	145.0
7	198.7	340.9	142.2	-0.37	139.7
8	233.3	336.7	103.4	-0.26	136.4
9	216.6 224.5	344.4	127.8	-0.34	122.3
paramylon	–	269.6	–	-2.34	–

3.2. Thermal analyses

Prior to melt spinning, we examined the thermal properties (T_m, *Td*5, T_g, and MVR) of the solid polysaccharide mixed esters prepared by the ethanol precipitation method.

3.2.1. Melting point

Fig. 1a shows the DSC thermograms (first heating scan) of **1a**−**9**. All the paramylon mixed esters exhibited T_m values ranging from ~190 to 250 °C (Table 2). The thermograms of **1b**−**7** show only endothermic peaks. The thermogram of **1a** differs from those of the other paramylon mixed esters in terms of the appearance of a distinct exothermic peak at 215.3 °C. Since exothermic peaks correspond to cold crystallization occurring during the heating process, cold crystallization is also thought to contribute partially to the endothermic peaks (Gan et al., 2017; Marubayashi et al., 2014; Mujica-Garcia et al., 2016). Fig. 2 shows the WAXD diffractogram of the ethanol-precipitated solid of **1a**. The appearance of some sharp diffraction peaks in the 2θ range from ~10 to 25° and broad halos in the higher-angle region indicate the coexistence of crystalline and amorphous phases. The thermogram of **8** shows not only an endothermic peak but also an exothermic one at 173.7 °C, similar to that of **1a**. The thermogram of **9** shows two endothermic peaks at 216.6 and 224.5 °C comparable to **1a**. No exothermic peak appears despite structural similarities to **1a** in terms of DS values.

3.2.2. Td5 and isothermal stability

*Td*5 is a typical index for evaluating resistance to heat degradation (Chen et al., 2010; Goto et al., 2000; Sato et al., 2014). Based on the *Td*5 of paramylon (~270 °C), the products can be categorized into three groups based on their *Td*5: (1) **1a–1c**, **2**, **3**, **5–9** with *Td*5 values higher than that of paramylon; (2) **1d** with *Td*5 comparable to that of paramylon; and (3) **4a** and **4b** with *Td*5 values lower than that of paramylon (Table 2). Hence, resistance to heat degradation apparently depends significantly on the chain length and DS of the acyl groups. *Td*5s of **8** and **9** are comparable to that of the structurally analogous **1a**. Another index for heat resistance is isothermal stability; degradation of the solids is evaluated by continuously measuring the sample weight loss percentage upon heating at 246 ± 1.0 °C for 30 min. These incubation temperature and period are supposedly close to those required for the actual practical operation. The weight loss percentages indicate that all the polysaccharides, except for **1d**, **4a**, and **4b**, show higher isothermal stabilities with weight loss less than 1.0% upon heating (Table 2). No significant difference in isothermal stability was observed between **1a** and its analogues (**8**, **9**).

For successful melt spinning, the extruding temperature must be lower than the decomposition temperature to avoid charring. In addition,

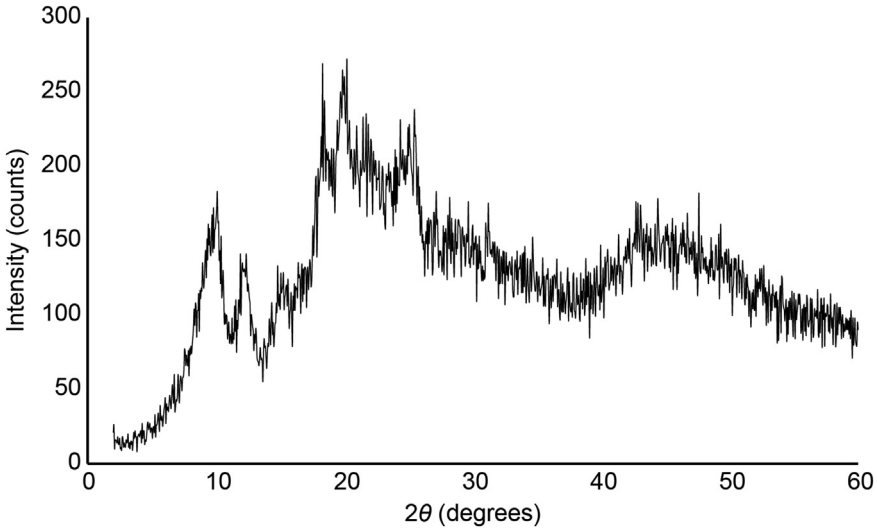

Fig. 2. WAXD pattern of ethanol-precipitated solids of **1a**.

the wider the process window ranging from the melting temperature to the decomposition temperature, the easier is the melt spinning operation. Hence, we used the difference between T*d*5 and T_m (i.e., T*d*5 − T_m) as the evaluation index. As shown in Table 2, the (T*d*5 − T_m) values are as large as 100 °C, except for **1c**, **1d**, **4a**, and **4b**.

3.2.3. Glass transition temperature

Fig. 1b shows the DSC curves (second heating scan) of **1a**−**9**. Apparently, T_gs are confirmed for all the compounds. A comparison of the T_g values of the paramylon acetate propionates (**1a**–**1d**) synthesized from acetic acid and propionic anhydride reveals that the higher the DS_{ace} (i.e., the lower the DS_{mc}), the higher is the T_g (Table 2). Since the polymer–polymer distance decreases with decreasing DS_{mc} of the propionyl group, this trend seems reasonable. The T_g values of the paramylon acetate propionates, prepared from propionic acid and acetic anhydride (**4a** and **4b**, respectively), are higher than those of **1a**−**1c** and are comparable to that of **1d**. The higher T_gs of **1d**, **4a**, and **4b** are due to their small polymer–polymer distances, as suggested by their higher DS_{ace} and lower DS_{mc} than those of **1a–1c**.

The similar DS values of **2** and **3** allow the effect of the chain length on T_g to be explicitly examined. For instance, a single methylene elongation induces a reduction in T_g as large as 14 °C. A comparison of the T_gs of **6** and **7**, which have similar DS values, suggests that the longer the medium-chain acyl group, the lower is the T_g. The increase in chain length of the medium-chain acyl group from butyryl (**5**) to pentanoyl (**6**) is not responsible for the decrease in T_g; rather, this is probably ascribable to the stronger polymer–polymer interactions in **6** than those in **5**, because the DS_{ace} and DS_{mc} of **6** are larger and smaller, respectively, than those of **5**. The T_g values suggest that all the paramylon mixed esters can form melt-spun filaments with thermostability comparable to those of the petroleum-based amorphous polymers, including polystyrene and polycarbonate (T_g = ~100 and ~139 °C, respectively), if they are successfully melt-spun (Claudy et al., 1983; Shamim et al., 2014).

The T_g of **8** (136.4 °C) is ~16 °C higher than that of **1a**, a structural analogue of **8** in terms of acyl chain length, DS, and molecular weight; this is attributable to the difference in glycosidic linkage (β-1,3 for **1a** vs β-1,4 for **8**). The compatibility of T_g between **1a** and **9** is reasonable because they are both β-1,3-glucan-based mixed esters with the same acyl group combination with close DS values.

3.2.4. Exothermic phenomena

Fig. 1b shows that two exothermic peaks appear at 162.9 °C and 199.9 °C in the curve for **1a** and one at 163.4 °C in that for **1b**. Given that the exothermic peaks are due to cold crystallization (Gan et al., 2017;

Table 3
Thermal properties of polysaccharide mixed esters.

Product	MVR (cm^3/10 min)								
	210 °C	220 °C		230 °C		240 °C		250 °C	
	98.07 (N)	37.26 (N)	98.07 (N)	37.26 (N)	98.07 (N)	37.26 (N)	98.07 (N)	37.26 (N)	98.07 (N)
1a	NE[a]	ND[b]	NE	ND	10.2	3.6	26.8	ND	ND
1b	ND	NE	NE	ND	6.7	3.5	28.5	>305.3[c]	ND
1c	ND	ND	ND	ND	ND	ND	1.7	66.4	277.5
1d	ND	ND	ND	ND	ND	7.7	5.8	ND	ND
2	ND	N.E.	2.0	1.2	15.9	20.2	ND	ND	ND
3	4.1	1.1	27.3	2.5	39.1	ND	ND	ND	ND
4a	ND	ND	ND	ND	ND	ND	NE	~~ND~~	2.2
4b	ND	ND	ND	ND	ND	ND	NE	ND	2.8
5	NE	ND	NE	ND	NE	8.6	22.8	ND	ND
6	ND	ND	ND	ND	1.7	>305.3	>305.3	>305.3	ND
7	NE	ND	0.7	ND	3.2	4.0	62.3	ND	ND
8	ND	ND	ND	ND	ND	ND	NE	6.1	ND
9					NE	ND	NE	ND	NE
paramylon	–	–	–	–	–	–	–	–	–

[a] NE: not extruded.
[b] ND: not determined.
[c] extruded within ~1 s.

Table 4
Preparation conditions and mechanical properties of monofilaments fabricated from **1a**, **1b**, and CAB.

Run	Product	Cylinder temperature (°C)	Extruding force (N)	Spinning rate (rpm)	Maximum strength (cN/dtex)	Elongation at break (%)	Resistance (cN/dtex)	Young's modulus (MPa)
1	**1a**	240	98.07	80	1.6 ± 0.7	28.8 ± 4.7	10.7 ± 3.6	1386.4 ± 470.2
2	**1a**	240	98.07	100	2.8 ± 1.0	28.2 ± 3.3	14.8 ± 7.5	1920.3 ± 968.8
3	**1a**	240	98.07	110	2.1 ± 0.9	26.6 ± 4.2	12.4 ± 5.5	1615.6 ± 714.8
4	**1b**	245	98.07	80	1.4 ± 0.5	27.1 ± 3.7	10.0 ± 2.3	1297.5 ± 304.7
5	**1b**	245	98.07	100	1.5 ± 0.3	25.6 ± 2.6	10.2 ± 1.9	1326.3 ± 241.8
6	CAB	165	37.26	–*	0.5 ± 0.1	5.6 ± 1.1	14.4 ± 1.7	1865.5 ± 225.2

* Manual spinning (~50 cm/s).

Marubayashi et al., 2014; Mujica-Garcia et al., 2016), we think that **1a** undergoes polymorph transition during heating from ambient temperature to ~200 °C, while **1b** does not. The larger ΔH values of **1a** (3.85 and 4.91 J/g at 162.9 and 199.9 °C, respectively) than that of **1b** (0.37 J/g) suggests that the former contains larger amorphous phase than the latter. This is because the crystallization rate of **1a** is lower than the cooling rate (5.0 °C/min) and that of **1b** is comparable to the cooling rate; therefore, a large part of **1a** and **1b** in the melt state turned to amorphous and crystalline phases, respectively, upon cooling to ambient temperature. Since **1a** and **1b** have comparable molecular weights, these differences in the thermograms are probably due to the differences in the acylation degrees; in other words, the differences in DS_{ace} and DS_{mc} of only ~0.3 between **1a** and **1b** are large enough for inducing the differences in thermal behaviors. The degrees of acylation will be discussed in Section 3.7.

Thermograms of **1a** and **1b** show apparent endothermic peaks at 221.2 and 208.2 °C, respectively (Fig. 1b). One cannot say with conviction that melt-solidified **1a** and **1b** have high crystallinity based on the appearance of the large endothermic peaks alone, because cold recrystallization is a primary contributor to these peaks. Hence, we presume that both **1a** and **1b** can form crystalline filaments if successfully melt-spun, while the others cannot be spun. The thermogram of **8** shows a distinct endothermic peak at 234.4 °C, indicating that this compound is crystalline. No exothermic peak due to cold crystallization suggests that its crystallization was completed within the cooling process from 230 to 25 °C with a cooling rate of 5.0 °C/min during the first heating/cooling process. Thermogram of **9** shows broad and sharp exothermic peaks at 168.0 and 200.9 °C, respectively, and an endothermic peak at 222.4 °C. The similarity of thermogram profile between **1** and **9** suggests the similarity in their polymer packing in the solid state.

3.2.5. *Melt volume flow rate*

To determine whether the polysaccharide mixed esters are melt-spinnable using the custom-built melt spinning apparatus, we measured their MVRs using the melt indexer and weights employed for spinning, the results of which are listed in Table 3. We confirmed that **1a** and **1b** have higher MVRs and **1c** and **1d** have lower MVRs among the propionyl-rich paramylon acetate propionates. The difference is particularly pronounced when the paramylon mixed esters are subjected to extrusion using the 98.07-N weight at 240 °C. This is likely because **1a** and **1b** have longer polymer–polymer distances than **1c** and **1d**, as indicated by their lower DS_{ace} and higher DS_{mc} values. Products **2** and **3** show higher MVR values than **1a** and **1b** due to the more pronounced thermoplasticization effect of the butanoyl and pentanoyl groups than that of the propionyl group. Compounds **4a** and **4b** are hardly extruded under the experimental conditions because of their high T_m above ~245 °C; the charred state of their filaments extruded at 250 °C is reasonable, given their negative ($Td5 - T_m$) indices (Table 2). Interestingly, although **5**–**7** show lower MVRs than **1a** and **1b** at 230 °C, **5** becomes as thermoplastic as **1a** and **1b**, and **6** and **7** become even more thermoplastic when the temperature is increased to 240 °C and a force of 98.07 N is used. This result suggests that the thermoplasticization effects of medium-chain acyl groups (butanoyl, pentanoyl, and hexanoyl) become apparent above a threshold temperature and force. Compound **8** shows lower MVR value than the structurally analogous **1a** probably due to the β-1,4-linkage in the main chain. Compound **9** was not extruded under the present experimental conditions due to its rather larger molecular weight than **1a** (Table 1).

3.3. *Melt spinnabilities*

Prior to mechanical spinning, we examined the spinnabilities of all the compounds using manual spinning (spinning rate of ~50 cm/s) as a preliminary experiment using the custom-built melt spinning apparatus. Since the speed of manual spinning can be adjusted, facilitating a balance between the extruded volume of the melted solid and that of the spun filament for avoiding filament breakage, we consider this a useful means for evaluating the melt spinnability of filament materials than the mechanical spinning performed at a constant speed. The cylinder temperature and weight were set by reference to the T_m and MVR results to gain expected the MVR values of 10–100 cm^3/10 min, which are roughly equivalent to or larger than the volumes of melt-spun filaments with a diameter of ~200 μm, e.g. cylinder temperature of 240 °C and 98.07-N weight for **1a**. The manual spinning test confirmed that filaments longer than a few meters were produced from **1a** and **1b**; in contrast, only fragile and/or short filaments of length less than a dozen centimeters

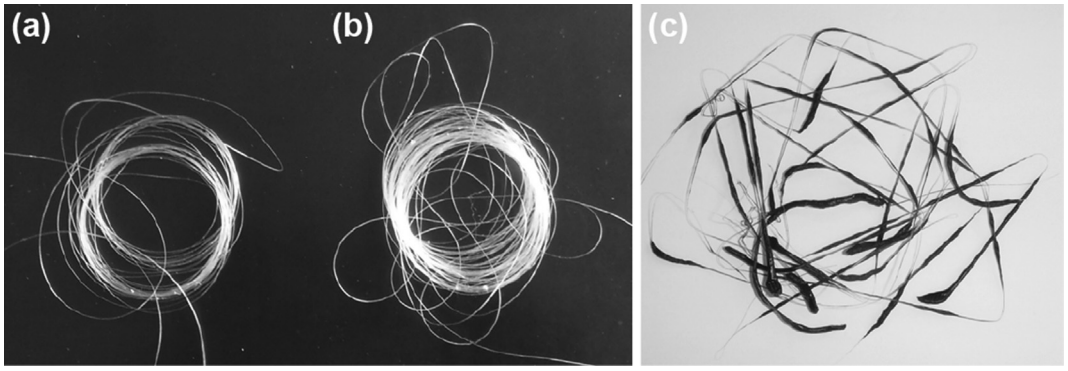

Fig. 3. Monofilaments of (a) **1a** (Run 1), (b) **1b** (Run 2), and (c) **8** produced by manual spinning (250 °C).

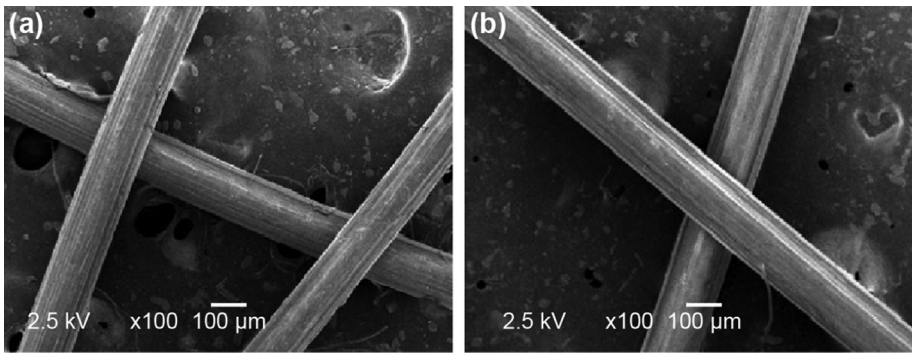

Fig. 4. SEM images of monofilaments of (a) **1a** (Run 1) and (b) **1b** (Run 4). Scale bar: 100 μm.

were obtained from **1c**−**3**, **5**–**8** and no filaments were obtained from **4a**, **4b**, and **9**, despite several attempts using different combinations of cylinder temperature, weight, and spinning rate. Hence, we chose **1a** and **1b** as the most promising filament materials among the paramylon mixed esters studied and subjected them to mechanical melt spinning.

Table 4 shows the spinning conditions used, i.e. the cylinder temperature, extruding force, and spinning rate. The cylinder temperature was set 15–20 °C higher than the T_m of the corresponding solid, enough for melting it inside the cylinder within 3 min. Since the cylinder temperature was ~100 °C lower than the T*d*5 value, polymer decomposition during the spinning process was negligible. Owing to mechanical limitations, the forces used herein for extrusion (98.07 N) were significantly lower than those employed for regular laboratory-scale melt spinning using a twin-screw microcompounder (4000–5000 N) (Hooshmand et al., 2014). The spinning rate, therefore, was decreased to 80–110 rpm (24–33 m/min), equivalent to the manual spinning rate; minor variation in spinning rate is needed to strike an optimum balance between the extruded volume of the melted solid and that of the spun filament, as attained in the manual spinning experiment.

We confirmed that under the spinning conditions listed in Table 4, long and fine monofilaments were produced from **1a** and **1b** (Fig. 3a and b). Fig. 4 shows the typical magnified SEM images of the melt-spun

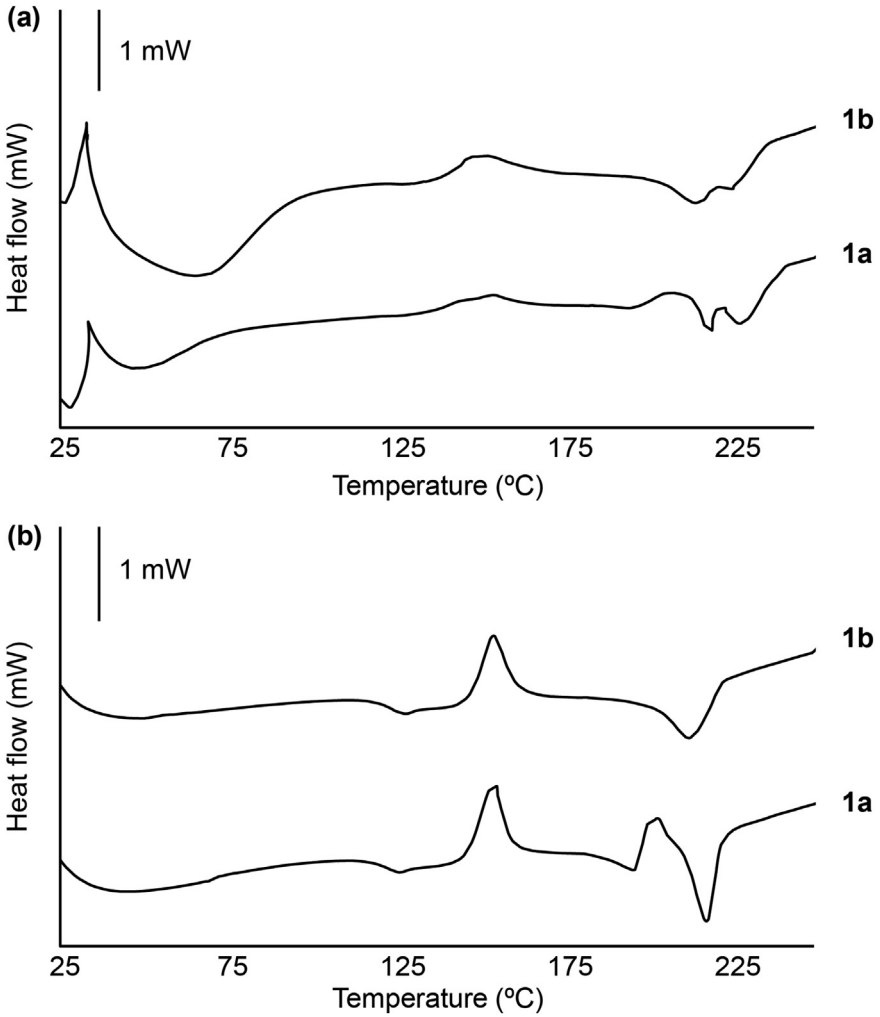

Fig. 5. DSC thermograms of monofilaments of **1a** (Run 1) and **1b** (Run 4): (a) first and second heating scans.

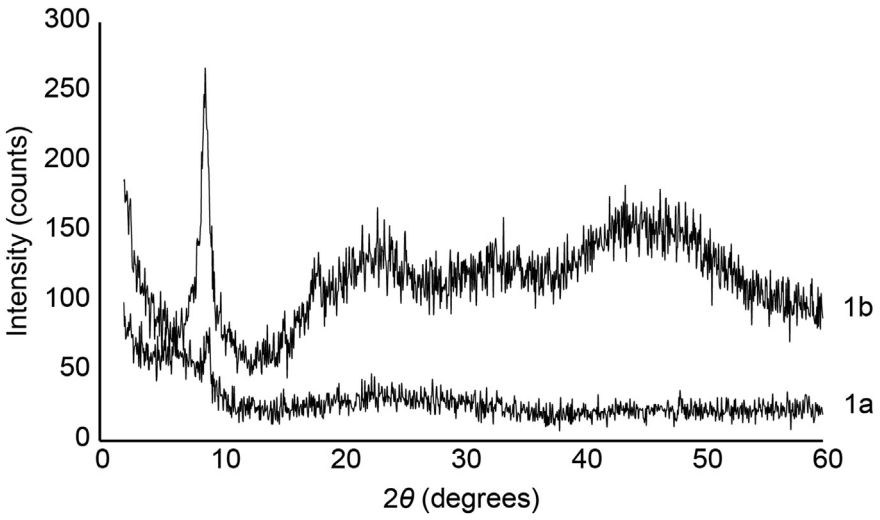

Fig. 6. WAXD patterns of monofilaments of **1a** (Run 1) and **1b** (Run 4).

filament surfaces, indicating that the filaments have uniform diameters, with no significant defects or roughness.

Table 4 also shows that the mechanical properties (maximum strength, elongation at break, and Young's modulus) of the spun monofilaments. There are no significant differences in the maximum strengths, resistances, and Young's moduli among the filaments spun from each product obtained at different spinning rates (Runs 1–3 for **1a** and Runs 4 and 5 for **1b**). Comparison between the **1a** and **1b** filaments reveals that the filaments spun from **1b** have slightly lower maximum strength, resistance, and Young's modulus than those spun from **1a**. Notably, since the properties of melt-spun filaments strictly depend on various spinning conditions, including shear rate of melted polymers, spinneret temperature, spinning rate, and cooling temperature, the mechanical properties listed in Table 3 do not weigh the relative merits of **1a** and **1b** as a filament material.

Solid **8** was unsuccessfully extruded using a cylinder temperature of 240 °C and a weight of 98.07 N, the same melt spinning conditions used for **1a** (Table 4). Increasing the cylinder temperature from 240 to 250 °C enabled extrusion of **8** through the spinneret, but only brittle, charred, and short filaments were produced by manual spinning (Fig. 3c). These results indicate that **8** is less suitable for melt spinning than **1a**, although **8** is a structural analogue of **1a**. Instead, monofilaments spun from commercially available CAB were prepared by manual spinning, because mechanical spinning produced broken filaments due to the high spinning rate and tension. While the CAB is not a strict control because its molecular weight is 10 times lower than that of **1a** and it has a different acyl group combination from **1a**, comparison of the mechanical properties between the **1a**/**1b** filaments and the CAB filaments indicates that filaments of **1a** and **1b** have mechanical properties comparable to those of the cellulose-based one obtained using melt spinning. Notably, the maximum strength of melt-spun filaments of **1a** and **1b** is comparable to that of cellulose acetate (CA) fibers (1.47–3.54 cN/dtex), spun from lyotropic crystals using the liquid crystal spinning method. This is useful for producing fibers with high breaking strength and high Young's modulus (Kamide, 2005), suggesting that the paramylon acetate propionate-based filaments can be put to practical use. We supposed that the high maximum strength stems from the crystalline nature of the filaments. Their crystallinity will be discussed in Section 3.5.

3.4. DSC analysis of monofilaments of paramylon acetate propionates

To gain further insight into the properties of the filaments melt-spun from **1a** and **1b**, we subjected them to DSC analysis. Fig. 5a shows the DSC profiles (first heating scan) of the filaments. The first heating scan of **1a**, which is representative for examining the thermal properties of melt-spun filaments (Mujica-Garcia et al., 2016), shows that two broad exothermic peaks with ΔH = 5.0 and 3.2 J/g, appearing at 153.5 and 207.0 °C, respectively, indicating that cold crystallization occurs in the filament as in the ethanol-precipitated and melt-solidified solids (Fig. 2). Two sharp exothermic peaks appear at 154.1 and 201.6 °C with ΔH of 9.0 and 5.6 J/g, respectively, during the second heating scan (Fig. 5b). The difference in exothermic peak width between the first and second heating scans is primarily attributable to the test sample form. In other words, roughly even heat-transfer distribution to the melt-solidified sample sealed in an aluminum pan induces cold recrystallization within a narrower temperature range to give sharp exothermic peaks (second scan), but cold recrystallization in the filamentary sample upon uneven heat-transfer distribution results in broader peaks (first scan). The differences in peak appearance can also be attributed to the lower crystallinity of the filament produced by quick cooling and higher crystallinity of the melt-solidified solid prepared by gradual cooling. The first and second heating scans of **1b** show broad and sharp exothermic peak at 152.4 and 154.3 °C with ΔH of 7.5 and 8.5 J/g, respectively. The difference in exothermic peak width between the two peaks can be rationally accountable for by the same reasons as the **1a** thermogram. Taken together, the DSC thermograms of the filaments indicate that the melt-spun filaments have crystalline character, albeit low in degree.

3.5. WAXD analysis of monofilaments of paramylon acetate propionates

DSC analysis indicated that the melt-spun filaments of **1a** and **1b** can have crystalline character. To examine this idea, they were subjected to WAXD analysis. Fig. 6 shows the diffractograms of the **1a** and **1b** filaments. A sharp peak in the low-angle region (i.e., at ~9°) and broad halos in the higher-angle region (i.e., >20°) in both diffractograms indicate the formation of the periodic structure of the paramylon backbone (Gan et al., 2017), suggesting that partial crystallization progresses during melt spinning. Based on the relative height of the sharp peaks at ~9°, crystallinity of the **1b** filament is plausibly higher than that of **1a** one. The solid **1b** has higher melt velocity than **1a**, suggested by a large difference in MVR values at the same temperature and weight as those used for each melt spinning process (i.e., 26.8 and 105.3 cm^3/10 min for **1a** and **1b**, respectively). This allows **1b** to gain higher polymer movement freedom and more time for recrystallization than **1a** during the quenched solidification process. We also assumed that the higher degree of acetylation of **1b** than that of **1a** facilitates crystallization, as suggested by the lower ΔH values of the exothermic and endothermic peaks of the **1b** thermogram (Fig. 1b). Although we do not seek for further reasons

underlying the crystallinity difference, in this study, various spinning conditions cooperatively control the filament properties. Taken together, the WAXD and DSC results confirmed that both **1a** and **1b** can form crystalline filaments.

3.6. DMA analysis of monofilaments of paramylon acetate propionates

Fig. 7 shows representative curves for the storage modulus (E'), loss modulus (E"), and tan δ of the monofilaments spun from **1a** (Run 1), **1b** (Run 4), and CAB. The storage moduli of the filaments of **1a** and **1b** gradually decrease with increasing temperature up to ~120 °C;

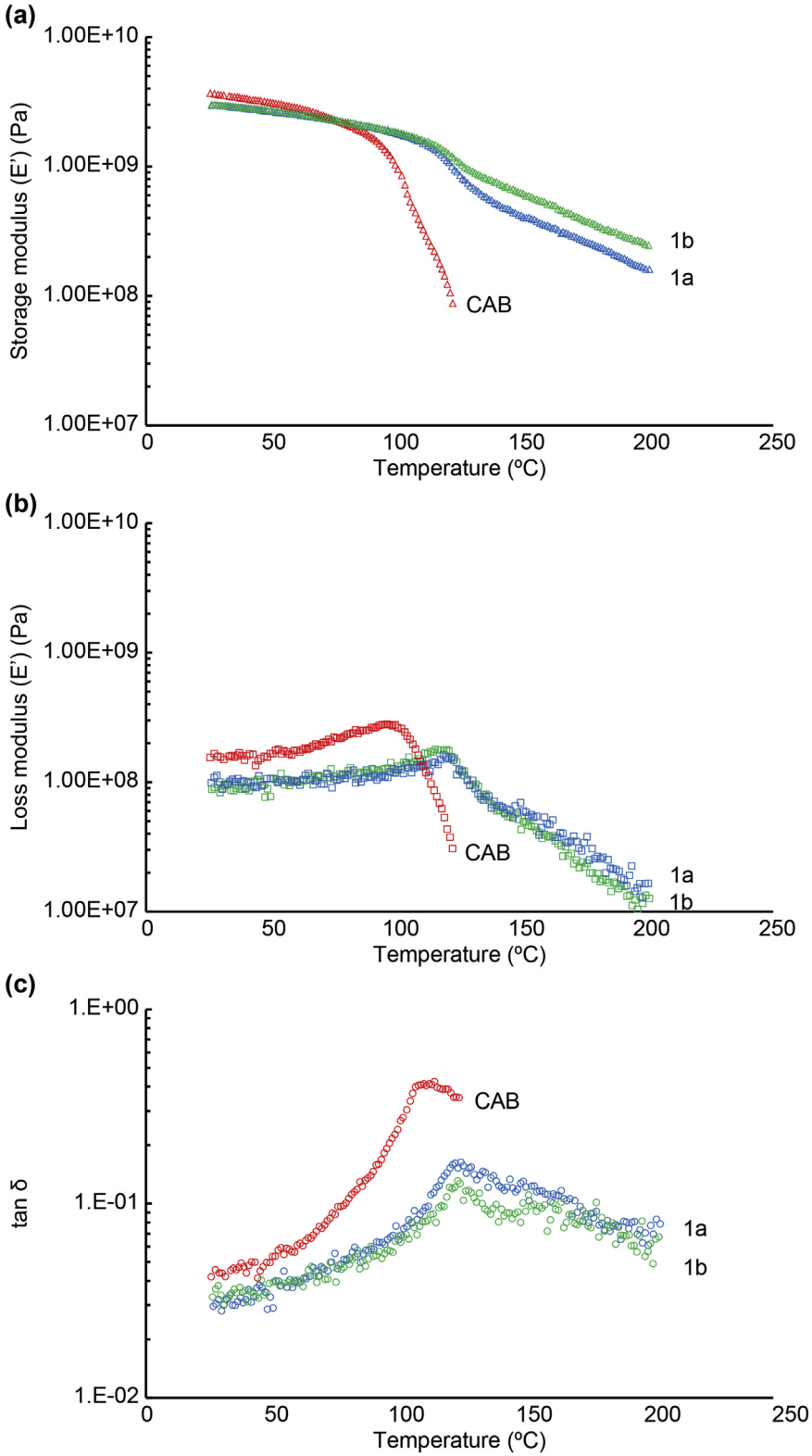

Fig. 7. Dependence of viscoelastic parameters on temperature; (a) storage moduli, (b) loss moduli, and (c) tan δ of 1a (Run 1), 1b (Run 4), and CAB.

Table 5
Storage modulus (E') of monofilaments.

Product	Storage modulus (E′) (MPa)			
	50 °C	100 °C	150 °C	200 °C
1a	2660	1780	404	160
1b	2720	1860	614	245
CAB	3090	952	–	–

thereafter, the storage moduli decrease much steeply (Fig. 7a). Since their tan δ curves show maxima around 120 °C (Fig. 7c), the glassy states of **1a** and **1b** probably change to the rubber state around this temperature. Comparison between **1a** and **1b** reveals that a significant difference in storage modulus becomes pronounced above ~120 °C (Fig. 7a). The storage moduli at different temperatures are shown in Table 5. The storage modulus of **1b** is ~1.5 times higher than that of **1a** at 150 and 200 °C. Since the molecular weights of **1a** and **1b** were similar, this result suggested that the degree of polymer entanglement in the **1b** filament is higher than that in the **1a** filament. No significant difference in loss modulus between **1a** and **1b** was observed over the measurement temperature range (Fig. 7b). The loss modulus curves of **1a** and **1b** show maxima at ~120 °C, as observed in the tan δ ones. These temperatures are defined as T_g, as determined by DMA, and are comparable to the T_g values determined by DSC.

The storage modulus of CAB is comparable to those of **1a** and **1b** at temperatures below ~90 °C, and thereafter it becomes smaller than those of **1a** and **1b**, and the measurement was terminated at ~120 °C because of the sample break (Fig. 7a, Table 5). Since the T_g determined by DSC of CAB is 97.1 °C, comparable to the T_g determined based on its loss modulus and tan δ curves (Fig. 7b and c), this rapid drop in storage modulus of CAB is ascribable to the transition from glassy state to rubber state. The larger rapid descent in the storage modulus of CAB than those of **1a** and **1b** is probably due to the higher thermal vibration of the butanoyl group as compared to those of acetyl and propionyl groups and the lower molecular weights of CAB than those of n**1a** and **1b**.

3.7. Chemical structures of the paramylon acetate propionates

As described above, **1a** and **1b** show differences in thermal behaviors, filament crystallinities, and mechanical properties at temperatures above T_g. Given the same acyl group combination and the close similarities of molecular weights between two compounds, the slight differences in acylation degree (~0.3) apparently induce these differences in physical properties. To gain insight into the chemical structural difference between them in terms of acyl substituents, acyl group distribution in the glucose unit was determined by quantitative ^{13}C NMR spectroscopy.

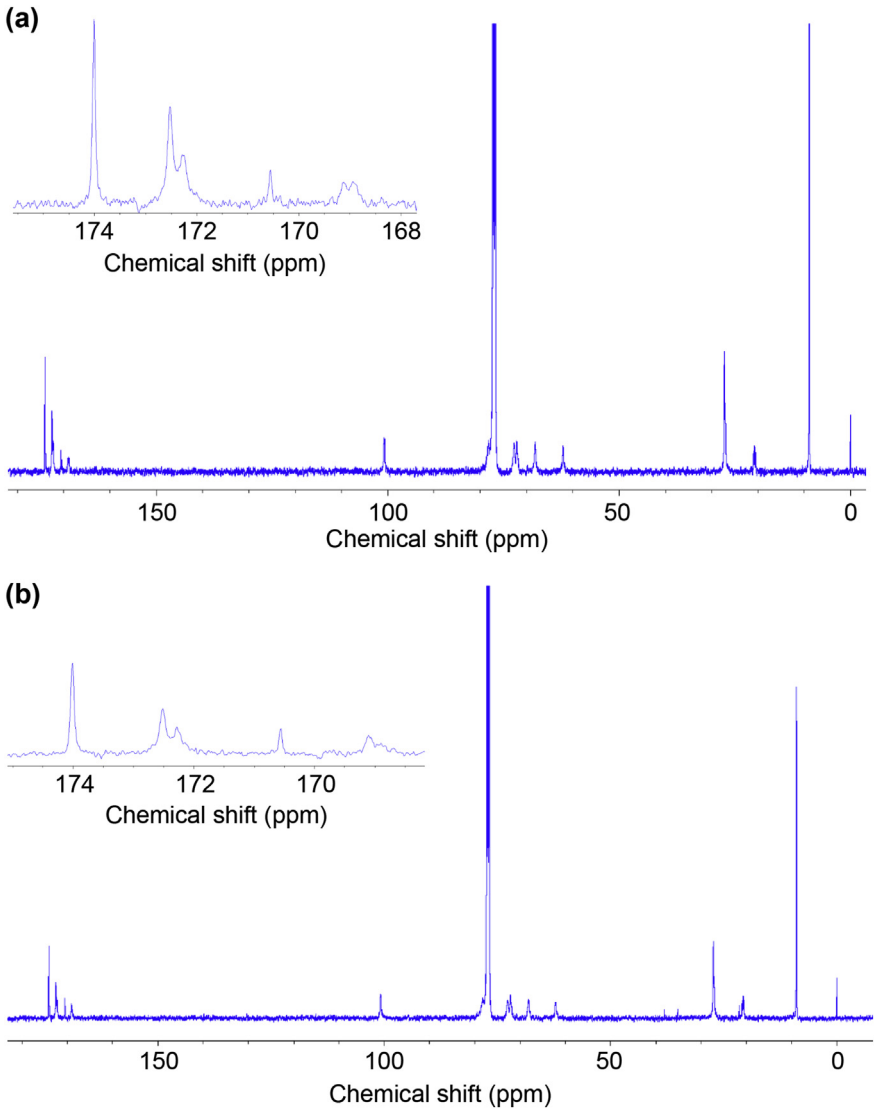

Fig. 8. Quantitative ^{13}C NMR spectra of (a) **1a** and (b) **1b**; the insets show the corresponding magnified spectra in the range 168–174 ppm.

Fig. 8 shows their ^{13}C NMR spectra (quantitative mode) and magnified views showing carbonyl carbon signals. Carbonyl carbon signals are sensitive NMR probes for monitoring substitution positions on a glucose unit (M. Shibakami, Tsubouchi and Hayashi, 2014; Motonari Shibakami, Tsubouchi, Sohma and Hayashi, 2015; Tezuka, 1993; Tezuka et al., 1991; Tezuka and Tsuchiya, 1995). Signals in the ranges 174−172 and 171−169 ppm are ascribed to the propionyl and acetyl carbons, respectively. Sharp signals at 174.0 and 170.6 ppm are due to the acyl groups at the C6 position. Broader signals at 173.0–172.0 and 169.5–168.5 ppm can be assigned to the acyl groups attached to the C2 and C4 positions, respectively. The overlapping peaks were deconvoluted using the Bruker Topspin software. Based on the relative integral values of the ^{13}C signals in each range and DS values listed in Table 1, distribution of each acyl group over three hydroxyl positions in a glucose residue was calculated as partial DS values (Table 6).

The average carbon numbers in the acyl chain of the glucose residue are 2.85 (= (0.46 × 2 + 2.54 × 3) ÷ 3) and 2.72 (= (0.72 × 2 + 2.24 × 3) ÷ 3) for **1a** and **1b**, respectively. Comparison of the partial DS values (Table 6) reveals that while the C4 position has less tendency to be propionylated and slightly greater preference for acetylation, each acyl group is nearly evenly introduced to the C2, C4, and C6 positions. The polymer chain packing in paramylon monoesters becomes more loose with increasing acyl chain length (Gan et al., 2019). Compounds **1a** and **1b** are considered structurally close to paramylon monoesters because there is a difference of only one carbon between the acetyl and propionyl groups. If that is the case, this result indicates that only a small difference in the average carbon number (2.85–2.72 = 0.13) is enough for inducing the differences in thermal, mechanical, and crystalline properties of the paramylon-based crystalline monofilaments.

Table 6
Partial degrees of substitution of acyl groups in **1a** and **1b**.

Product	Partial DS_{ace}			Partial DS_{mc}		
	C2	C4	C6	C2	C4	C6
1a	0.11 (4)*	0.20 (6)	0.15 (5)	0.89 (30)	0.72 (24)	0.93 (31)
1b	0.23 (8)	0.28 (9)	0.21 (7)	0.75 (25)	0.62 (21)	0.87 (30)

* Values in parentheses indicate the percentage of substituent occupancy in a glucose residue.

4. Conclusions

We examined the suitability of melt spinning for the preparation of monofilaments from paramylon mixed esters. We found that paramylon acetate propionates having DS_{ace} values of 0.5–0.7 and DS_{mc} values of 2.2–2.5 are melt-spinnable. Their monofilaments are mechanically tough, making them easy to handle, probably due to their high DPs (~1500) and their crystalline nature. In contrast, melt spinning of cellulose acetate propionate and curdlan acetate propionate, structural analogues of the melt-spinnable paramylon acetate propionates, did not produce continuous filaments. Considering their unsuccessful melt spinning, the melt spinnabilities of the paramylon acetate propionates are primarily explained based on their higher thermoplasticities than these structural analogues. In addition, our process avoids the use of solvent and plasticizers. These results support our hypothesis that thermoplastic paramylon mixed esters can be transformed more readily into mechanically robust monofilaments than the structurally analogous cellulose and curdlan derivatives, if their physical properties and spinning conditions are well-matched. Experiments for developing applications for these monofilaments are currently underway. Nonetheless, these paramylon-based monofilaments can be used in medical materials, such as sutures, because of their mechanical toughness, potential biodegradability, and biocompatibility.

Declarations

Author contribution statement

Motonari Shibakami: Conceived and designed the experiments; Performed the experiments; Analyzed and interpreted the data; Contributed reagents, materials, analysis tools or data; Wrote the paper.

Mitsugu Sohma, Norihito Kijima: Performed the experiments; Analyzed and interpreted the data; Contributed reagents, materials, analysis tools or data.

Tadashi Nemoto: Analyzed and interpreted the data.

Funding statement

This research did not receive any specific grant from funding agencies in the public, commercial, or not-for-profit sectors.

Competing interest statement

The authors declare no conflict of interest.

Additional information

Supplementary content related to this article has been published online at https://doi.org/10.1016/j.heliyon.2019.e02843.

Acknowledgements

The authors are grateful to KOBELCO Eco-Solutions Co., Ltd. for providing paramylon. We are also grateful to Mr. Yasushiro Otsuka (TA Instruments Japan Inc.) for his technical assistance with DMA.

References

Aranishi, Y., Yamada, H., Maeda, Y., Takahashi, H., Ozaki, M., Nishio, Y., Yoshioka, M., 2006. US Patent 06984631.

Chen, J.-L., Jin, F.-L., Park, S.-J., 2010. Thermal stability and impact and flexural properties of epoxy resins/epoxidized castor oil/nano-$CaCO_3$ ternary systems. Macromol. Res. 18 (9), 862–867.

Claudy, P., Létoffé, J.M., Camberlain, Y., Pascault, J.P., 1983. Glass transition of polystyrene versus molecular weight. Polym. Bull. 9 (4), 208–215.

Erdmann, R., Kabasci, S., Kurek, J., Zepnik, S., 2014. Study of reactive melt processing behavior of externally plasticized cellulose acetate in presence of isocyanate. Materials 7 (12), 7752–7769.

Gan, H., Enomoto, Y., Kabe, T., Ishii, D., Hikima, T., Takata, M., Iwata, T., 2017. Synthesis, properties and molecular conformation of paramylon ester derivatives. Polym. Degrad. Stab. 145, 142–149.

Gan, H., Kabe, T., Kimura, S., Hikima, T., Takata, M., Iwata, T., 2019. Crystal structures and crystalline elastic modulus of paramylon esters. Polymer 172, 7–12.

Goto, K., Kakuta, M., Inoue, Y., Matsubara, M., 2000. Low dielectric and thermal stable polyimides with fluorene structure. J. Photopolym. Sci. Technol. 13 (2), 313–315.

Hooshmand, S., Aitomäki, Y., Skrifvars, M., Mathew, A.P., Oksman, K., 2014. All-cellulose nanocomposite fibers produced by melt spinning cellulose acetate butyrate and cellulose nanocrystals. Cellulose 21 (4), 2665–2678.

Kamide, K., 2005. 3 - molecular properties of cellulose and cellulose derivatives. In: Kamide, K. (Ed.), Cellulose and Cellulose Derivatives. Elsevier, Amsterdam, pp. 189–444.

Marubayashi, H., Yukinaka, K., Enomoto-Rogers, Y., Takemura, A., Iwata, T., 2014. Curdlan ester derivatives: synthesis, structure, and properties. Carbohydr. Polym. 103, 427–433.

Mujica-Garcia, A., Hooshmand, S., Skrifvars, M., Kenny, J.M., Oksman, K., Peponi, L., 2016. Poly(lactic acid) melt-spun fibers reinforced with functionalized cellulose nanocrystals. RSC Adv. 6 (11), 9221–9231.

Nakagawa, T., 1952a. Spinnability of liquid. A visco-elastic state. I. Spinnability and anomalous viscosity. Bull. Chem. Soc. Jpn. 25 (2), 88–93.

Nakagawa, T., 1952b. Spinnability of liquid. A visco-elastic state. II. Spinnability and visco-elastic property. Bull. Chem. Soc. Jpn. 25 (2), 93–97.

Park, H.-M., Misra, M., Drzal, L.T., Mohanty, A.K., 2004. "Green" nanocomposites from cellulose acetate bioplastic and clay: effect of eco-friendly triethyl citrate plasticizer. Biomacromolecules 5 (6), 2281–2288.

Puanglek, S., Kimura, S., Iwata, T., 2017. Thermal and mechanical properties of tailor-made unbranched α-1,3-glucan esters with various carboxylic acid chain length. Carbohydr. Polym. 169, 245–254.

Savage, A.B., Young, A.E., Maasberg, A.T., 1954. Cellulose and Cellulose Derivatives, second ed., V. Interscience Publishers Inc, New York.

Sato, E., Taniguchi, K., Inui, T., Yamanishi, K., Horibe, H., Matsumoto, A., 2014. Dismantling behavior of pressure sensitive adhesives using acrylic block and random copolymers in response to photoirradiation and postbaking. J. Photopolym. Sci. Technol. 27 (4), 531–534.

Shibakami, M., Sohma, M., 2017. Synthesis and thermal properties of paramylon mixed esters and optical, mechanical, and crystal properties of their hot-pressed films. Carbohydr. Polym. 155, 416–424.

Shamim, N., Koh, Y., Simon, S., McKenna, G., 2014. Glass transition temperature of thin polycarbonate films measured by flash differential scanning calorimetry. J. Polym. Sci., Part B: Polym. Phys. 52, 1462–1468.

Shibakami, M., Tsubouchi, G., Hayashi, M., 2014. Thermoplasticization of euglenoid beta-1,3-glucans by mixed esterification. Carbohydr. Polym. 105, 90–96.

Shibakami, M., Tsubouchi, G., Sohma, M., Hayashi, M., 2015. One-pot synthesis of thermoplastic mixed paramylon esters using trifluoroacetic anhydride. Carbohydr. Polym. 119, 1–7.

Teramoto, Y., 2015. Functional thermoplastic materials from derivatives of cellulose and related structural polysaccharides. Molecules 20 (4), 5487–5527.

Tezuka, Y., 1993. 13C NMR determination of the distribution of two ester substituents in cellulose acetate butyrate. Carbohydr. Res. 241 (0), 285–290.

Tezuka, Y., Imai, K., Oshima, M., Ito, K.-i., 1991. 13C-N.m.r. structural study on an enteric pharmaceutical coating cellulose derivative having ether and ester substituents. Carbohydr. Res. 222 (0), 255–259.

Tezuka, Y., Tsuchiya, Y., 1995. Determination of substituent distribution in cellulose acetate by means of a 13C NMR study on its propanoated derivative. Carbohydr. Res. 273 (1), 83–91.

Throne, J.L., 2008. Polymers and plastics. In: Throne, J.L. (Ed.), Understanding Thermoforming, second ed. Hanser, pp. 171–204.

Toyama, K., Soyama, M., Tanaka, S., Iji, M., 2015. Development of cardanol-bonded cellulose thermoplastics: high productivity achieved in two-step heterogeneous process. Cellulose 22 (3), 1625–1639.

Zepnik, S., Kabasci, S., Kopitzky, R., Radusch, H.-J., Wodke, T., 2013. Extensional flow properties of externally plasticized cellulose acetate: influence of plasticizer content. Polymers 5 (3), 873–889.